A&A 493, 445–451 (2009)
DOI: 10.1051/0004-6361:200809665

Astronomy & Astrophysics

An extreme EXO: a type 2 QSO at $z = 1.87$

A. Del Moro[1], M. G. Watson[1], S. Mateos[1], M. Akiyama[2], Y. Hashimoto[3], N. Tamura[4], K. Ohta[5], F. J. Carrera[6], and G. Stewart[1]

[1] XROA-University of Leicester, University Road, Leicester LE1 7RH, UK
e-mail: ad187@star.le.ac.uk
[2] Astronomical Institute, Tohoku University, Sendai 980-8578, Japan
[3] South African Astronomical Observatory, Observatory Road, Cape Town 7539, South Africa
[4] Subaru Telescope, National Astronomical Observatory of Japan, Hilo, HI 96720, Japan
[5] Department of Astronomy, Kyoto University, Kyoto 606-8502, Japan
[6] Instituto de Física de Cantabria (CSIC-UC), Avenida de los Castros, 39005 Santander, Spain

Receievd 27 February 2008 / Accepted 23 September 2008

ABSTRACT

Aims. We aim to understand the multi-wavelength properties of 2XMM J123204+215255, the source with the most extreme X-ray-to-optical flux ratio amongst a sample of bright X-ray selected EXOs drawn from a cross-correlation of the 2XMMp catalogue with the SDSS-DR5 catalogue.
Methods. We use 2XMMp X-ray data, SDSS-DR5, NOT and UKIRT optical/NIR photometric data and Subaru MOIRCS IR spectroscopy to study the properties of 2XMM J123204+215255. We created a model SED including an obscured QSO and the host galaxy component to constrain the optical/IR extinction and the relative contribution of the AGN and the galaxy to the total emission.
Results. 2XMM J123204+215255 is a bright X-ray source with $f_X \approx 10^{-12}$ erg cm^{-2} s^{-1} (2–10 keV energy band) which has no detection down to a magnitude $i' > 25.2$. NIR imaging reveals a faint K-band counterpart and NIR spectroscopy shows a single broad ($FWHM \simeq 5300$ km s^{-1}) emission line, which is almost certainly Hα at $z = 1.87$. The X-ray spectrum shows evidence of significant absorption ($N_H > 10^{23}$ cm^{-2}), typical of type 2 AGN, but the broad Hα emission suggests a type 1 AGN classification. The very red optical/NIR colours ($i' - K > 5.3$) strongly suggest significant reddening however. We find that simple modelling can successfully reproduce the NIR continuum and strongly constrain the intrinsic nuclear optical/IR extinction to $A_V \approx 4$, which turns out to be much smaller than the expected from the X-ray absorption (assuming Galactic gas-to-dust ratio).

Key words. galaxies: active – galaxies: quasars: general – X-rays: galaxies – infrared: galaxies

1. Introduction

Over the past few years, extensive studies have been carried out to determine the complete census of the active galactic nuclei (AGN) population, in particular the bright, obscured objects (optically type 2 QSOs), invoked by the synthesis models of the X-ray background (XRB, Setti & Woltjer 1989; Comastri et al. 1995; Comastri 2001; Gilli et al. 2001, 2007). The deepest surveys carried out to date by *Chandra* and XMM-Newton have resolved >90% (Mushotzky et al. 2000; Hasinger et al. 2001; Alexander et al. 2003) of the XRB spectrum at energies below 5 keV, however a large number of the obscured AGN are still missing. For these reasons, many studies have been addressed to reveal this elusive class of objects, primarily focused on the X-ray band, but also involving multi-wavelength studies (Zakamska et al. 2003, 2004; Martínez-Sansigre et al. 2006).

In previous studies, the X-ray-to-optical-flux ratio (f_X/f_{opt}[1]), defined here as the ratio between the X-ray flux (usually in the 2–10 keV energy band) and R-band flux, has been commonly used to provide a first classification of the X-ray population (Maccacaro et al. 1988): normal galaxies have typically $f_X/f_{opt} \lesssim 0.1$ (e.g. Giacconi et al. 2001; Lehmann et al. 2001) while the dominant X-ray selected AGN population has $0.1 < f_X/f_{opt} < 10$ (e.g. Akiyama et al. 2000; Alexander et al. 2001; Fiore et al. 2003); obscured AGN typically have $f_X/f_{opt} \sim 10$ or above (e.g. Mignoli et al. 2004).

Recently, a new interesting class of objects with extreme values of the X-ray-to-optical flux ratio ($f_X/f_{opt} > 10$) has been found from deep X-ray surveys; these objects, called *Extreme X-ray-to-Optical ratio sources* (EXOs, Koekemoer et al. 2004), are usually detected in X-rays and in near-IR, but completely undetected in the optical bands. Although a few turn out to be BL Lac objects, high-redshift clusters of galaxies or rare Galactic objects (e.g. X-ray binaries, cataclysmic variables, isolated neutron stars or ultraluminous X-ray sources), the majority are almost certainly type 2 AGN (Fiore et al. 2003), where the nucleus is heavily obscured by dust in the UV/optical/IR whilst the X-ray flux, although strongly absorbed at low energies (below ~2 keV), is much less affected by absorption above ~2 keV.

As expected in this scenario, a significant fraction of the EXO population shows the extremely red colours of EROs (*extremely red objects*, typical $R - K \geq 5$, Elston et al. 1988; see Fiore et al. 2003; Mignoli et al. 2004). EXOs with optical-NIR colours of EROs are thus amongst the best candidates to be highly absorbed, highly obscured AGN, i.e. type 2 AGN.

However, almost by definition, sources with such extreme f_X/f_{opt} have faint optical magnitudes and this is even more true for the faint X-ray sources found in the deep, pencil-beam surveys (Koekemoer et al. 2004; Civano et al. 2005). At such faint

[1] f_X/f_{opt} is defined here as $\log(f_X/f_{opt}) = \log f_{2-10\,keV} + r'/2.5 + 5.5$ (e.g. Civano et al. 2005), where $f_{2-10\,keV}$ is the X-ray flux (erg cm^{-2} s^{-1}) and r' is the Sloan magnitude in the r' band (AB).

X-ray fluxes ($f_X = 10^{-15}$–10^{-16} erg cm^{-2} s^{-1}), sources with $f_X/f_{opt} > 10$ have R magnitudes ~25.5–28, so the optical follow-up observations are very difficult or impossible. Studies performed at higher X-ray fluxes ($f_X = 10^{-14}$–10^{-13} erg cm^{-2} s^{-1}, e.g. Fiore et al. 2003; Mignoli et al. 2004; Severgnini et al. 2006), for which optical data are available, have classified more than a half of their EXO sources as type 2 QSOs.

In this paper, we report the results obtained from the multi-wavelength analysis of 2XMM J123204+215255, the most extreme source amongst a sample of 130 bright ($f_X \geq 10^{-13}$ erg cm^{-2} s^{-1}) X-ray selected EXOs (Del Moro et al., in prep.) from the 2XMMp catalogue (the pre-release of the Second XMM-Newton Serendipitous Source Catalogue, Watson et al. 2008). The whole sample is described in Sect. 2.1. The X-ray and optical/NIR properties of 2XMM J123204+215255 are discussed in Sects. 2.2 and 2.3, respectively; a detailed description of the NIR spectrum is presented in Sect. 2.4. An SED model analysis and results are discussed in Sect. 3, followed by the conclusions (Sect. 4). Throughout the paper we assume a cosmological model with $H_0 = 70$ km s^{-1} Mpc^{-1}, $\Omega_M = 0.27$ and $\Omega_\Lambda = 0.73$ (Spergel et al. 2003).

2. Observations and results

2.1. The EXO sample

The object we present in this paper is part of a sample selected from a cross-correlation between the 2XMMp[2] and the *Sloan Digital Sky Survey, Data Release 5* (SDSS-DR5, Adelman-McCarthy et al. 2007) catalogues, which yields about 20 000 secure matches. SDSS optical counterparts have been selected on the basis of positional matching, using an adaptation of the *likelihood ratio* method (e.g. Sutherland & Saunders 1992) to optimise the choice of correct counterpart and minimise the contamination by chance matches. Full details of our approach will appear in Del Moro et al., in preparation.

Our sample consists of relatively bright X-ray sources with $f_X \geq 10^{-13}$ erg cm^{-2} s^{-1} (0.2–12 keV energy band) and extreme X-ray-to-optical flux ratio ($f_X/f_{opt} > 10$, in the 2–10 keV band). Each XMM and SDSS image of the sample objects has been carefully checked by eye in order to reject all the problematic cases: spurious X-ray detections, sources close to the edge of the XMM-Newton field of view, extended X-ray sources[3], optical counterparts in big nearby galaxies (HII region emissions). Because we are selecting extreme X-ray-to-optical flux ratio objects, the counterparts of our sources are typically faint in the optical, at our sensitivity limits, making it difficult in some cases to differentiate between the possibility that the true match is fainter than the SDSS limit or that the correct counterpart is a faint object with low likelihood ratio (and hence with a higher probability to be a chance match). The effects of this ambiguity are that the f_X/f_{opt} values, in these cases, will be *underestimated* (i.e. if the counterpart is fainter than the SDSS limit). In this sense our sample is robust.

The sample resulting from these selection processes consists of 130 sources for which ~30% (including 2XMM J123204+215255) have no optical counterpart in the SDSS imaging data within 7″ from the X-ray position (see Sect. 2.2), down to a magnitude limit of $r' = 22.5$.

2.2. X-ray properties of 2XMM J123204+215255

The source 2XMM J123204+215255 is the most extreme X-ray-to-optical flux ratio object amongst our EXO sample. It is a bright X-ray source with $f_X = 8.8^{+0.7}_{-2.6} \times 10^{-13}$ erg cm^{-2} s^{-1} (in the 2–10 keV energy band). On the basis of the lack of an SDSS counterpart it has $f_X/f_{opt} > 278$, already one of the highest ratios recorded, whilst as we show below, new data demonstrate the ratio to be $f_X/f_{opt} > 3300$, making it the highest known X-ray-to-optical flux ratio source outside the Galaxy. The source has been detected in an XMM-Newton observation with target "NGP Rift 3" which was made in July 2001 with an exposure time of ~15 ks with pn and ~20 ks with MOS1 and MOS2.

The statistical position error for 2XMM J123204+215255 is 0.3″. Taking into account the expected systematic error component for the 2XMMp catalogue of 0.35″, determined from a comparison of catalogue positions with the SDSS-DR5 Quasar Catalog (see Watson et al. 2008), we expect the counterpart to lie within ≈1.4″ (99% confidence). The comparison with the SDSS Quasar Catalog shows that there are a very small number of outliers at larger separations in excess of what is expected statistically (presumably indicating a larger systematic error component in these rare cases), but in no case the separation is >7 arcsec. We adopt this value as the most conservative upper limit on the possible separation of the true counterpart.

To study the X-ray spectrum of 2XMM J123204+215255, the data have been processed using the standard SAS v.7.1.0 tasks (XMM-Newton Science Analysis System, Gabriel et al. 2004). We extracted the spectrum of the source using an elliptical region to reproduce the shape of the Point Spread Function (PSF) of the XMM Telescopes at the source position. The corresponding background spectrum has been extracted using an annular region with radii 30″ and 90″, centred on the source position, removing any other detected nearby sources. The data have been then filtered for high background intervals. The total EPIC number of counts in the 0.2–12 keV energy band after the filtering is 2234. The spectral analysis has been performed with XSPEC v.11.3.2 (Arnaud 1996), grouping the number of counts to a minimum of 10 counts per bin, in order to use the χ^2 statistic. We find an acceptable fit to a simple model composed of a power-law plus Galactic and intrinsic absorptions; fixing $N_H^{gal} = 2 \times 10^{20}$ cm^{-2}, the best fit parameters are photon index $\Gamma = 1.7 \pm 0.2$ and hydrogen column density $N_H = (1.2 \pm 0.2) \times 10^{22}$ cm^{-2} (assuming $z = 0$), with χ^2/d.o.f. = 118.0/106.

Repeating the X-ray spectral analysis for $z = 1.87$, anticipating the result presented below (Sect. 2.4), we obtained a best fit to the data with a photon index $\Gamma = 1.5 \pm 0.1$ and a column density $N_H = (1.8 \pm 0.3) \times 10^{23}$ cm^{-2} (Fig. 1). We note the presence of marginally significant structure in the spectrum residuals at energy ~1.5–3 keV which might be related to red-shifted line or edge features. The reality of these features clearly require confirmation at higher signal-to-noise.

2.3. Optical/IR properties

As noted above (Sect. 2.1), there is no counterpart for 2XMM J123204+215255 in SDSS DR5 within 7″ (Sect. 2.2) from the X-ray position in any of the SDSS bands (u', g', r', i', z',

[2] Although this object was originally selected from the 2XMMp, we adopt the nomenclature and catalogue parameters from the 2XMM catalogue throughout as 2XMM effectively supersedes 2XMMp.

[3] As we are looking for AGN, we want to select only X-ray point-like sources in our sample, so extended sources are considered as "problematic cases" amongst our selection criteria.

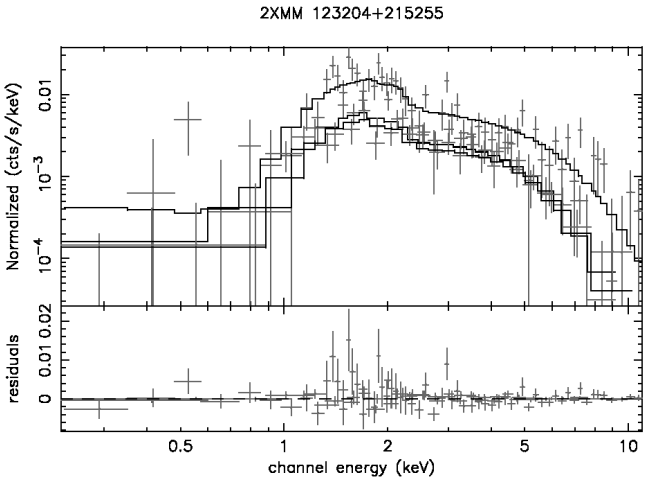

Fig. 1. EPIC pn, MOS1 and MOS2 X-ray spectrum of 2XMM J123204+215255 (*top panel*): the model is represented by the black lines; residuals are also shown (*lower panel*). The data are well represented by an absorbed power-law with a photon index $\Gamma = 1.5 \pm 0.1$ and a hydrogen column density $N_{\rm H} = 1.8 \times 10^{23}$ cm^{-2} at $z = 1.87$.

Fukugita et al. 1996), indeed the nearest SDSS object lies ∼30″ away.

We obtained deeper optical imaging of the field on 2007 February 9 on the 2.5 m NOT (*Nordic Optical Telescope*). Four separate i'-band images were taken with the NOT ALFOSC camera with integration times of 1800 s each. Conditions were photometric with ∼1 arcsec seeing, but unfortunately the images are affected by bad fringing. As there were no sky flats available to correct properly for the fringing, an empirical approach was adopted in which a smoothed version of each image (with bright objects removed) is used to estimate the effective sky background plus fringing effects. The resultant background-subtracted images were then stacked to make the final image (Fig. 2). This technique does not fully remove the fringing effects, but reduces them to a modest level, significantly improving the sensitivity for faint objects.

We find no detection of any counterpart within 7 arcsec of the position of 2XMM J123204+215255 with an estimated 5σ limit $i' > 25.2$ mag, based on the amplitude of the residual background fluctuations. The photometric calibration was established by comparing the count rates of a sample of objects detected in the NOT image with the SDSS-DR5 photometric catalogue.

As the object is likely to be heavily obscured in the optical, the obvious next step is IR observations, where the effective dust obscuration will be lower. Follow-up J-band and K-band observations of 2XMM J123204+215255 have been obtained with the *UK Infrared Telescope-Wide Field Infrared Camera* (UKIRT-WFCAM) the 12th of February 2007 with an exposure time of 1200 s in the J-band and 2×1200 s in the K-band. The IR images (Fig. 2) show an apparently stellar counterpart in the K-band with a magnitude $K = 18.0 \pm 0.05$ (Vega, $K = 19.9 \pm 0.05$ in AB magnitude system, Oke & Gunn 1983; see Hewett et al. 2006) and a very marginal detection in the J-band ($J \gtrsim 21.3$, Vega). All the values are reported in Table 1. The IR counterpart lies ≈1″ from the X-ray centroid, consistent with the position errors discussed in Sect. 2.2. The IR detection allows us to place limits on the optical/IR colours of the source: $r' - K > 2.6$ and $i' - K > 5.3$ (AB). As the optical emission is likely to be dominated by a high redshift galaxy, as discussed below, it is likely that $r' - i' > 0$, which means that the r' magnitude should be of the order of $r' \gtrsim 25.2$. If that is true, the $r' - K$ colour becomes greater than 5.3 (AB), corresponding to $r' - K > 7$ in the Vega system, which is extremely red even for EROs (Sect. 1).

2.4. IR spectrum

2XMM J123204+215255 was observed in the $H + K$ bands with the *Multi-Object Infrared Camera and Spectrograph* (MOIRCS, Ichikawa et al. 2006) at the Subaru Telescope in March 2007. The observation was performed in long-slit spectroscopy mode using the $HK500$ grism and 0.8″ slit width, under a seeing of 0.6″. The spectrum covers a wavelength range of 13 000–23 000 Å with a spectral resolution of ≈40 Å (∼5 pix) *FWHM* estimated from the width of OH airglow lines.

We took 6 target frames with 7 min exposure each, thus the total on-source integration time was 42 min. The telescope was dithered after every single exposure and the target was observed at different positions along the slit (1.5″ or 3″ from the slit centre). After sky subtraction, carried out by subtracting adjacent object frames from each other, flat-fielding was performed using dome-flat frames. These sky-subtracted and flat-fielded frames were then shifted, mirrored and combined to determine the average intensity value at each pixel with a 3σ clipping algorithm. Atmospheric absorption correction and flux calibration have been performed using the spectrum of a bright star (HD 119496, spectral type of A2V). The standard star spectrum was taken at the end of the night at a similar airmass to the target and with the same instrumental setup.

The observed spectrum (Fig. 3) reveals a red continuum emission, which is well represented by $f_\lambda \propto \lambda$. Using this form and extrapolating it out to the wavelengths longer than 23 000 Å, the K-band magnitude of this source is estimated to be 19.7 ± 0.1 mag in the AB system without any corrections (the emission line is at the edge of the K-band and its effect on this estimate can be ignored). This is consistent with the UKIRT-WFCAM photometry ($K = 19.9 \pm 0.05$, see Sect. 2.3 and Table 1) within the uncertainties. An estimated ∼10% of the total flux from the object falls outside the slit width in the 0.6″ seeing conditions of the observation. As the slit losses are uncertain and the magnitude estimates from the spectroscopy are consistent with the UKIRT imaging, we therefore do not apply any slit-loss corrections to the emission line fluxes estimated below, but note that they have ∼10–20% systematic uncertainty.

As shown in Fig. 3, a single broad emission line ($FWHM = 5280 \pm 331$ km s^{-1}) is clearly visible on the red continuum in the observed spectrum at 18837 ± 7 Å (line centroid). The line flux is $f = (5 \pm 0.2) \times 10^{-16}$ erg cm^{-2} s^{-1} (uncorrected for absorption; Table 2). The emission line centre and line width have been estimated by fitting a Gaussian to the spectrum in the vicinity of the line after the continuum was subtracted, whilst the line flux was estimated by directly integrating the continuum-subtracted line profile. The derived *Equivalent Width* (EW) is $EW = 2500 \pm 140$ Å. All the uncertainties are estimated from the 1σ errors in the Gaussian fitting process.

Although there are no other significant emission or absorption lines visible in the spectrum, the most likely interpretation is that the line detected is Hα. We also considered other possible interpretations for this line:

i) if it were one of the Paschen series the implied redshift would be $z < 1$ which seems unlikely as the host galaxy is not detected in the optical (and would thus be a very low luminosity object) and the detected line flux would be much higher than expected;

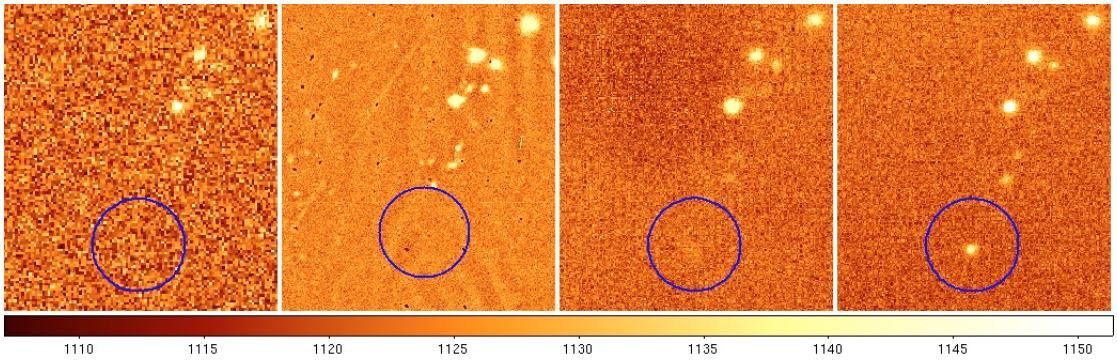

Fig. 2. Optical/IR finding charts for 2XMM J123204+215255. *From left to right*: SDSS r'-band image, NOT i'-band stacked image, UKIRT-WFCAM J and K bands. The K-band image shows an apparently stellar counterpart ($K = 19.9, AB$). The circles have a radius of 7″ and are centred on the X-ray position.

Table 1. Multi-wavelength properties of 2XMM J123204+215255.

IAU Name	RA Dec [h:m:s][d:m:s]	EPIC cts[a]	$f_{2-10\,\mathrm{keV}}$ [10^{-13} erg cm^{-2} s^{-1}]	$L_{2-10\,\mathrm{keV}}$ [10^{46} erg s^{-1}]	f_X/f_{opt}	r'[b] [mag]	i'[c] [mag]	J[d] [mag]	K[d] [mag]
2XMM J123204+215255	12:32:04.91+21:52:55.4	2234	$8.8^{+0.7}_{-2.6}$	1.6	>278 (>3300)*	>22.5	>25.2	>22.2	19.9

[a] Total pn+MOS1+MOS2 counts. [b] SDSS (AB). [c] NOT (AB). [d] UKIRT-WFCAM (AB). * Expected value derived from i-band limit, see text.

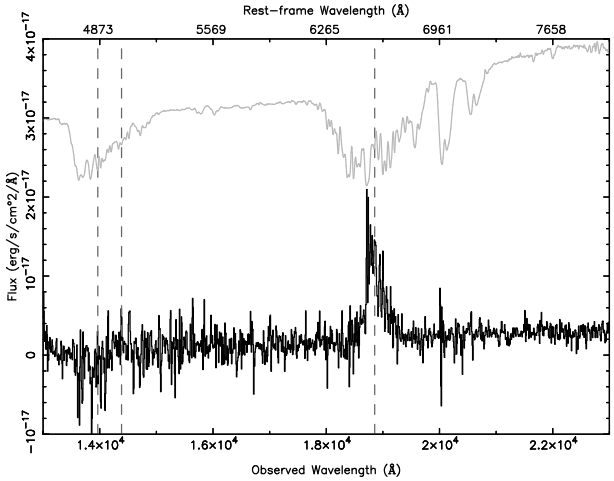

Fig. 3. The Subaru MOIRCS IR spectrum of 2XMM J123204+215255 (black) showing a single broad emission line ($FWHM = 5280 \pm 331$ km s^{-1}), likely to be Hα at $z = 1.87$. The grey spectrum shows the ratio between raw and final flux-calibrated spectrum. The ratio is dominated by the effects of atmospheric absorption and thus provides an indication of the main regions where such features are significant. The dashed vertical lines indicate the central wavelengths of Hα (see Sect. 2.4) and the expected Hβ and [OIII] emission lines for this redshift. *On the top axis* the rest-frame wavelengths are plotted.

ii) if it were MgII the redshift would be $z \sim 5.7$ which would make the X-ray absorption $N_H \approx 1.5 \times 10^{24}$ cm^{-2} (Compton thick). However, no strong Fe Kα line is detected in the X-ray spectrum and the derived luminosity at this redshift is extremely high ($L_X \approx 1.8 \times 10^{47}$ erg s^{-1}), so we believe also this hypothesis is unlikely.

Assuming the Hα identification is correct, the estimated redshift for the source is $z = 1.87$. Even though the emission line is just at the wavelength range where the spectrum is seriously affected by the atmospheric absorption lines between H and K bands, this can not explain the total absence of the [OIII] (expected from the Narrow Line Region) and the Hβ emission lines. For those lines we estimate flux upper limits from our MOIRCS spectrum: $f_{[OIII]} < 3 \times 10^{-17}$ erg cm^{-2} s^{-1} (assuming an $FWHM \leq 500$ km s^{-1}) and $f_{H\beta} < 1 \times 10^{-16}$ erg cm^{-2} s^{-1} (assuming the same $FWHM$ as Hα). These limits are conservative values estimated at several times higher than the formal 3σ level (derived from empirical estimates of the noise in the vicinity of these lines) to allow for the systematic deviations from the expected smooth continuum. The estimated line ratio Hα/Hβ is >5, which is higher than the typical intrinsic unreddened value for AGN (Hα/H$\beta \approx 3.5$, e.g. Ward et al. 1988). Noting that the Hβ flux is a conservative upper limit, this already indicates significant extinction in this object. We also note the clear asymmetry in the Hα line profile for which we have no obvious explanation, although an incomplete correction for the severe atmospheric absorption may be a possible reason. A narrow [N II] λ6583 line may also be present in the spectrum and contribute to the asymmetry of the Hα profile. The presence of this line, assuming it has $FWHM \leq 500$ km s^{-1}, cannot however explain all the red wing, given the Hα line width.

3. Discussion

For a redshift $z = 1.87$, the intrinsic X-ray luminosity for the source is $L_X = 1.6 \times 10^{46}$ erg s^{-1} (2–10 keV rest-frame) and the X-ray spectrum has a large column density ($N_H \approx 2 \times 10^{23}$ cm^{-2}; Sect. 2.2). The X-ray properties of 2XMM J123204+215255 are thus those of a very luminous, heavily absorbed AGN, with spectral parameters typical for a type 2 QSO.

In contrast the IR spectrum shows a broad Hα emission line and the IR counterpart detected in the K-band has a probable stellar morphology, characteristics of a type 1 object. To further complicate the story the predicted emission line fluxes are much higher than those observed (see Table 2). Using the correlation between hard X-ray luminosities and Hα and [OIII] luminosities from Panessa et al. (2006):

$$\log L_X = (1.06 \pm 0.04) \log L_{H\alpha} + (-1.14 \pm 1.78)$$
$$\log L_X = (1.22 \pm 0.06) \log L_{[OIII]} + (-7.34 \pm 2.53)$$

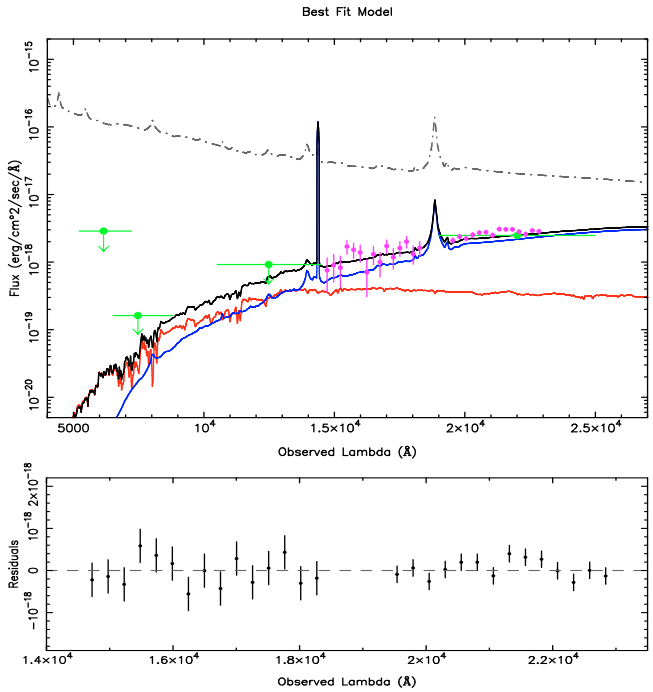

Fig. 4. Best-fit model of the NIR spectrum (magenta points); green circles: photometric measurements and upperlimits of the r', i', J and K-band magnitudes; red line: galaxy SED; blue line: absorbed QSO SED; grey dash-dotted line: unabsorbed QSO SED; black line: resulting SED (QSO + host galaxy). In *the lower panel* the residuals of the fitting are shown.

Table 2. Observed and predicted line fluxes of 2XMM J123204+215255.

Line	Observed flux[a] [erg cm^{-2} s^{-1}]	Predicted flux[b] [erg cm^{-2} s^{-1}]	Corrected flux [erg cm^{-2} s^{-1}]	A_λ^c [mag]
Hα	$(5 \pm 0.2) \times 10^{-16}$	1.7×10^{-14}	4.6×10^{-15}	2.4
Hβ	$<1 \times 10^{-16}$	4.8×10^{-15}	–	5.3
[OIII]	$<3 \times 10^{-17}$	2.9×10^{-15}	–	–

[a] Uncorrected for extinction, measured from the IR spectrum.
[b] From the correlations of Panessa et al. (2006).
[c] Extinction estimated from the model.

the predicted flux for Hα is $f_{\mathrm{H}\alpha} \sim 1.7 \times 10^{-14}$ erg cm^{-2} s^{-1}, which is about 30 times higher than the detected line flux (uncorrected for absorption) and the predicted fluxes for [OIII] and Hβ are $f_{[\mathrm{OIII}]} \sim 2.9 \times 10^{-15}$ erg cm^{-2} s^{-1} and $f_{\mathrm{H}\beta} \sim 4.8 \times 10^{-15}$ erg cm^{-2} s^{-1} (assuming the standard Hα/Hβ ratio, e.g. Ward et al. 1988), whereas these lines are not detected at all.

In order to see whether it was possible to reconcile the X-ray, optical and near IR characteristics of this object, we carried out simple modelling of the IR spectral continuum using a composite Spectral Energy Distribution (SED) with two components: one corresponding to the host galaxy and one to a typical QSO (Fig. 4). As QSOs are typically found to be hosted by massive elliptical galaxies (McLeod & Rieke 1995; Aretxaga et al. 1998; Dunlop et al. 2003), we adopted a 5 Gyr early-type galaxy template, generated with the GRASIL code (Silva et al. 1998). To reproduce the QSO we adopted a composite spectrum of a type 1 QSO with the highest IR/optical ratio (from Polletta et al. 2007). In the model the QSO SED component has intrinsic absorption, i.e. nuclear extinction, parameterised by a rest-frame equivalent A_V and represented by the Small Magellanic Cloud (SMC) extinction curve from Pei (1992), whilst both the QSO and galaxy SEDs have fixed Galactic absorption ($N_{\mathrm{H}}^{\mathrm{gal}} = 2 \times 10^{20}$ cm^{-2}), using the Milky Way extinction curve (Pei 1992). The other free parameter in the model is the *Galaxy Fraction* (g), which we define as the ratio between the host galaxy and the intrinsic QSO fluxes in the rest-frame wavelength range $\lambda_1 = 4160$ Å $< \lambda < \lambda_2 = 4210$ Å, chosen because it avoids most of the galaxy absorption lines and the quasar emission lines (Vanden Berk et al. 2006), i.e.:

$$g = \frac{\int_{\lambda_1}^{\lambda_2} f_{\lambda,\mathrm{gal}}\, \mathrm{d}\lambda}{\int_{\lambda_1}^{\lambda_2} f_{\lambda,\ \mathrm{QSO}}\, \mathrm{d}\lambda}.$$

We used this SED model to fit the IR continuum (Fig. 3) in the wavelength range 14 500–23 000 Å. As we aimed to reproduce only the spectral continuum, we excluded the emission line from the fitting; we excluded also the wavelengths below 14 500 Å because of the lower S/N in this part of the spectrum and to avoid the wavelengths of the expected [OIII] and the Hβ emission lines. After binning the spectrum, we computed χ^2 values for a grid of possible nuclear extinction and *Galaxy Fraction* (g) parameters and we determined confidence intervals for the two free parameters using the usual $\Delta\chi^2$ prescription (Fig. 5). Our modelling provides strong constraints on the rest-frame equivalent $A_V = 3.2$–5.0 (90% confidence), while the galaxy contribution is not strongly constrained. The best-fit of the near IR spectrum and the residuals of the fitting are shown in Fig. 4. We can also use the model fit results to constrain the expected r', i' and J-band magnitudes. Our best-fit model predicts $r' \approx 27.7$, $i' \approx 26.3$ and $J \approx 22.6$, values consistent with the upper limits discussed in Sect. 2.3. We note that the general properties of 2XMM J123204+215255 are rather similar to the object presented by Severgnini et al. (2006), although our source has higher extinction and has not yet been detected in the optical band. Our constraints on the host galaxy mass are comparable to, or somewhat lower than, that inferred by Severgnini et al. (2006) for their object.

Our modelling cannot of course be considered as definitive, as it is limited by the restricted wavelength coverage of our data, by the fact that we cannot be sure of the intrinsic SEDs for the galaxy and AGN components and by the assumption that just two components will adequately represent the data. We can however examine how our results depends on the choice of the SED components in the spectral range we are investigating, by using different QSO templates (from Polletta et al. 2007) in the fitting process. For this range of templates we find variations of $\lesssim$10% in the derived rest-frame equivalent A_V. As in all the models we tested the contribution of the galaxy appears to be only few percent of the total emission there is clearly little sensitivity to the precise shape of the galaxy SED adopted.

With the model parameters obtained from our analysis, the extinction for the QSO component in the J-band (close to Hβ and [OIII]) corresponds to $\approx$5.3 mag and $\approx$2.4 mag in the K-band, in the vicinity of the redshifted Hα line. Correcting the observed Hα flux for this extinction (A_K) gives a value $f_{\mathrm{H}\alpha} \approx 4.6 \times 10^{-15}$ erg cm^{-2} s^{-1}, which is lower than the flux expected from the L_{X}–$L_{\mathrm{H}\alpha}$ correlation of Panessa et al. 2006 (see Table 2), but well within the scatter of the correlation. The much higher extinction ($A_J \approx 5.3$) at the Hβ line is fully consistent with its non-detection.

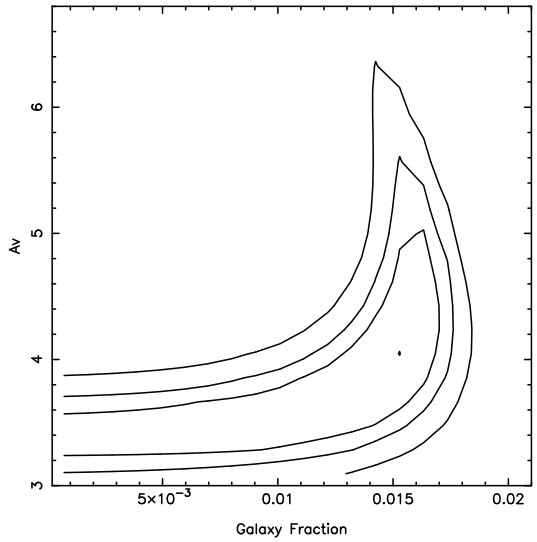

Fig. 5. χ^2 contours at 68, 90 and 99% confidence obtained from modelling of the IR spectrum for a grid of *Galaxy Fraction* and A_V values, as defined in the text.

The lack of detection of the [OIII] line is not explained in the model, as this line is expected to originate in the Narrow-Line Region (NLR) which should not be affected by the large extinction of the nuclear region. However, the weakness or disappearance of the [OIII] emission line has already been reported for high-luminosity AGN (see Yuan & Wills 2003; Netzer et al. 2004; Sulentic et al. 2004). A possible explanation may be related to the fact that the simple scaling law: $R_{\rm NLR} \propto L_{\rm ion}^{1/2}$ (where $R_{\rm NLR}$ is the radius of the Narrow Line Region and $L_{\rm ion}$ is the ionising source luminosity, Netzer et al. 2004), which may explain the correlation between the X-ray and the [OIII] luminosities at lower values, must break down when the NLR radius becomes comparable with the size of the galaxy.

Another possible explanation may be the presence of obscuring dust *outside* the torus, at larger distances from the nucleus. This dust could reside in the NLR (Polletta et al. 2008) or in the host galaxy (Rigby et al. 2006; Martínez-Sansigre et al. 2006; Brand et al. 2007) and could thus absorb the emission coming from the Narrow Line Region. This interpretation is equally consistent with the observed red continuum and the extinction of the broad lines whilst also providing an explanation for the absence of any narrow lines in the IR spectrum. However, as it is not possible to constrain the location of the obscuring dust with the present data, neither interpretation can be rejected.

Finally we note that the values obtained for the optical extinction from our modelling are significantly lower than naively expected from the measured X-ray column density. This can most easily be parameterised by a dust-to-gas ratio which is about 20–25 times lower than the standard Galactic value ($A_V = N_{\rm H}/(1.8 \times 10^{21})$, e.g. Predehl & Schmitt 1995). Such low ratios have been reported in several previous studies of AGN (Maccacaro et al. 1982; Maiolino et al. 2001b; Akiyama et al. 2002; Willott et al. 2004). In this comparison, as is the case in the other papers cited, we are assuming the simplest possible geometry where the dust and gas are co-spatial and lie in a uniform foreground screen[4]. One possible explanation for the high ratio is a different dust grain size distribution dominated by large grains, whose formation is naturally expected in the high density environments, like those characterising the circumnuclear region of AGNs. This dust grain distribution makes the extinction curve flatter than the Galactic one and yields a higher $N_{\rm H}/A_V$ ratio (Maiolino et al. 2001a; Maiolino 2002). This would not be a valid explanation if the absorption is on kpc-scales as discussed above.

4. Summary and conclusions

On the basis of its X-ray and optical properties, 2XMM J123204+215255 has the highest recorded $f_{\rm X}/f_{\rm opt}$ of any extragalactic X-ray source. IR spectroscopy confirms this object is an AGN at $z = 1.87$. In X-rays it is a very luminous object with large absorption, making it a type 2 QSO. Its optical/NIR properties show a strongly reddened continuum, but stellar appearance in the K band and broad Hα, more consistent with a type 1 classification (type 1.9 in the classification used for low redshift AGN). We have shown that these apparently discrepant properties can be reconciled with a model consisting of a heavily reddened AGN nucleus (rest-frame equivalent $A_V = 3.2–5.0$) and fainter host galaxy. Our results provide tight constrains on the X-ray column density and optical/IR extinction which demand a dust-to-gas ratio for this object ~25 times lower than the standard Galactic value. The non-detection of a narrow [OIII] emission line at anything like the expected flux in this object may be related to its very high luminosity.

Alternatively 2XMM J123204+215255 might be a member of a population of AGN with absorption on kpc-scales, sometimes described as "host-obscured" AGN (e.g. Brand et al. 2007), which may be an important ingredient in resolving the discrepancy between the predicted and observed ratios of type I and type II AGN, which exists in some models of AGN obscuration (e.g. Martínez-Sansigre et al. 2006; Brand et al. 2007).

We have shown that $f_{\rm X}/f_{\rm opt}$ selection using the large samples afforded by the 2XMM catalogue provides an effective way of discovering extreme objects like 2XMM J123204+215255, which are a rare but important part of the obscured AGN population. Our analysis has demonstrated that the extreme properties of this object are a natural consequence of its very high luminosity and large obscuration. It is interesting to note that a high luminosity object of this type with only a factor of a few higher absorption would appear as an entirely "normal" galaxy, in that it would have no detectable broad lines in its spectrum and presumably no narrow lines either, given the apparent strong suppression of the NLR emission lines evident at these high luminosities.

Acknowledgements. The data presented here include those taken using ALFOSC, which is owned by the Instituto de Astrofísica de Andalucía (IAA) and operated at the Nordic Optical Telescope under agreement between IAA and the NBIfAFG of the Astronomical Observatory of Copenhagen. The analysis in this paper are based in part on data collected at Subaru Telescope, which is operated by the National Astronomical Observatory of Japan. The United Kingdom Infrared Telescope is operated by the Joint Astronomy Centre on behalf of the Science and Technology Facilities Council of the UK. We gratefully acknowledge the SPARTAN support under the contract MEST-CT-2004-7512. F.J.C. acknowledges financial support by the Spanish Ministerio de Educación y Ciencia under project ESP2006-13608-C02-01. S.M. acknowledges direct support from the UK STFC research Council. We thank the referee for the constructive comments, which helped to improve the paper.

[4] This assumption may lead to an underestimation of the effective extinction of the source (e.g. MacKenty et al. 2000). More realistic dust and gas distributions can of course lead to different conclusions about the dust-to-gas ratio; however, as it is not possible to constrain the gas and dust distribution with the present data, considering more sophisticated models is beyond the purpose of our analysis.

References

Adelman-McCarthy, J. K., Agüeros, M. A., Allam, S. S., et al. 2007, ApJS, 172, 634
Akiyama, M., Ohta, K., Yamada, T., et al. 2000, ApJ, 532, 700
Akiyama, M., Ueda, Y., & Ohta, K. 2002, ApJ, 567, 42
Alexander, D. M., Brandt, W. N., Hornschemeier, A. E., et al. 2001, AJ, 122, 2156
Alexander, D. M., Bauer, F. E., Brandt, W. N., et al. 2003, AJ, 126, 539
Aretxaga, I., Terlevich, R. J., & Boyle, B. J. 1998, MNRAS, 296, 643
Arnaud, K. A. 1996, in Astronomical Data Analysis Software and Systems V, ed. G. H. Jacoby & J. Barnes, ASP Conf. Ser., 101, 17
Brand, K., Dey, A., Desai, V., et al. 2007, ApJ, 663, 204
Civano, F., Comastri, A., & Brusa, M. 2005, MNRAS, 358, 693
Comastri, A. 2001, X-ray Astronomy: Stellar Endpoints, AGN, and the Diffuse X-ray Background, AIP Conf. Proc., 599, 73
Comastri, A., Setti, G., Zamorani, G., & Hasinger, G. 1995, A&A, 296, 1
Dunlop, J. S., McLure, R. J., Kukula, M. J., et al. 2003, MNRAS, 340, 1095
Elston, R., Rieke, G. H., & Rieke, M. J. 1988, ApJ, 331, L77
Fiore, F., Brusa, M., Cocchia, F., et al. 2003, A&A, 409, 79
Fukugita, M., Ichikawa, T., Gunn, J. E., et al. 1996, AJ, 111, 1748
Gabriel, C., Denby, M., Fyfe, D. J., et al. 2004, in Astronomical Data Analysis Software and Systems (ADASS) XIII, ed. F. Ochsenbein, M. G. Allen, & D. Egret, ASP Conf. Ser., 314, 759
Giacconi, R., Rosati, P., Tozzi, P., et al. 2001, ApJ, 551, 624
Gilli, R., Salvati, M., & Hasinger, G. 2001, A&A, 366, 407
Gilli, R., Comastri, A., & Hasinger, G. 2007, A&A, 463, 79
Hasinger, G., Altieri, B., Arnaud, M., et al. 2001, A&A, 365, L45
Hewett, P. C., Warren, S. J., Leggett, S. K., & Hodgkin, S. T. 2006, MNRAS, 367, 454
Ichikawa, T., Suzuki, R., Tokoku, C., et al. 2006, in Ground-based and Airborne Instrumentation for Astronomy, ed. I. S. McLean, & M. Iye, Proc. SPIE, 6269, 626916
Koekemoer, A. M., Alexander, D. M., Bauer, F. E., et al. 2004, ApJ, 600, L123
Lehmann, I., Hasinger, G., Schmidt, M., et al. 2001, A&A, 371, 833
Maccacaro, T., Perola, G. C., & Elvis, M. 1982, ApJ, 257, 47
Maccacaro, T., Gioia, I. M., Wolter, A., Zamorani, G., & Stocke, J. T. 1988, ApJ, 326, 680
MacKenty, J. W., Maíz-Apellániz, J., Pickens, C. E., Norman, C. A., & Walborn, N. R. 2000, AJ, 120, 3007
Maiolino, R. 2002, in Issues in Unification of Active Galactic Nuclei, ed. R. Maiolino, A. Marconi, & N. Nagar, ASP Conf. Ser., 258, 15
Maiolino, R., Marconi, A., & Oliva, E. 2001a, A&A, 365, 37
Maiolino, R., Marconi, A., Salvati, M., et al. 2001b, A&A, 365, 28
Martínez-Sansigre, A., Rawlings, S., Lacy, M., et al. 2006, MNRAS, 370, 1479
McLeod, K. K., & Rieke, G. H. 1995, ApJ, 454, L77
Mignoli, M., Pozzetti, L., Comastri, A., et al. 2004, A&A, 418, 827
Mushotzky, R. F., Cowie, L. L., Barger, A. J., & Arnaud, K. A. 2000, Nature, 404, 459
Netzer, H., Shemmer, O., Maiolino, R., et al. 2004, ApJ, 614, 558
Oke, J. B., & Gunn, J. E. 1983, ApJ, 266, 713
Panessa, F., Bassani, L., Cappi, M., et al. 2006, A&A, 455, 173
Pei, Y. C. 1992, ApJ, 395, 130
Polletta, M., Tajer, M., Maraschi, L., et al. 2007, ApJ, 663, 81
Polletta, M., Weedman, D., Hönig, S., et al. 2008, ApJ, 675, 960
Predehl, P., & Schmitt, J. H. M. M. 1995, A&A, 293, 889
Rigby, J. R., Rieke, G. H., Donley, J. L., Alonso-Herrero, A., & Pérez-González, P. G. 2006, ApJ, 645, 115
Setti, G., & Woltjer, L. 1989, A&A, 224, L21
Severgnini, P., Caccianiga, A., Braito, V., et al. 2006, A&A, 451, 859
Silva, L., Granato, G. L., Bressan, A., & Danese, L. 1998, ApJ, 509, 103
Spergel, D. N., Verde, L., Peiris, H. V., et al. 2003, ApJS, 148, 175
Sulentic, J. W., Stirpe, G. M., Marziani, P., et al. 2004, A&A, 423, 121
Sutherland, W., & Saunders, W. 1992, MNRAS, 259, 413
Vanden Berk, D. E., Shen, J., Yip, C.-W., et al. 2006, AJ, 131, 84
Ward, M. J., Done, C., Fabian, A. C., Tennant, A. F., & Shafer, R. A. 1988, ApJ, 324, 767
Watson, M. G., Schröder, A. C., Fyfe, D., et al. 2008, ArXiv e-prints, 807
Willott, C. J., Simpson, C., Almaini, O., et al. 2004, ApJ, 610, 140
Yuan, M. J., & Wills, B. J. 2003, ApJ, 593, L11
Zakamska, N. L., Strauss, M. A., Krolik, J. H., et al. 2003, AJ, 126, 2125
Zakamska, N. L., Strauss, M. A., Heckman, T. M., Ivezić, Ž., & Krolik, J. H. 2004, AJ, 128, 1002